AGU PUBLICATIONS

Geophysical Research Letters

RESEARCH LETTER
10.1002/2015GL065228

Key Points:
- TGFs are produced when a lightning leader is near the midpoint of its ascent
- Lightning leaders associated with TGFs are fast moving but otherwise ordinary
- Why TGFs are not produced at other times in the leader ascent is not clear

Correspondence to:
Steven A. Cummer,
cummer@ee.duke.edu

Citation:
Cummer, S. A., F. Lyu, M. S. Briggs, G. Fitzpatrick, O. J. Roberts, and J. R. Dwyer (2015), Lightning leader altitude progression in terrestrial gamma-ray flashes, *Geophys. Res. Lett.*, *42*, doi:10.1002/2015GL065228.

Received 9 JUL 2015
Accepted 17 AUG 2015
Accepted article online 22 AUG 2015

Lightning leader altitude progression in terrestrial gamma-ray flashes

Steven A. Cummer[1], Fanchao Lyu[1], Michael S. Briggs[2], Gerard Fitzpatrick[3], Oliver J. Roberts[3], and Joseph R. Dwyer[4]

[1]Electrical and Computer Engineering Department, Duke University, Durham, North Carolina, USA, [2]CSPAR, University of Alabama in Huntsville, Huntsville, Alabama, USA, [3]School of Physics, University College Dublin, Dublin, Ireland, [4]Space Science Center (EOS) and Department of Physics, University of New Hampshire, Durham, New Hampshire, USA

Abstract Radio emissions continue to provide insight into the production of terrestrial gamma ray flashes (TGFs) by thunderstorms, including the critical question of the conditions under which they are generated. We have identified several TGF-associated lightning radio emissions in which the altitudes of in-cloud lightning leader pulses that precede and follow the TGF can be measured. We combine these with high absolute timing accuracy TGF observations from the Fermi satellite to determine the development of the lightning channel before, during, and after the TGF production. All of these TGFs were produced several milliseconds after the leader had initiated and when the leaders reached 1–2 km in length. After the TGFs, the leaders all continued to ascend for several more kilometers with no dramatic change in their characteristics, although they all exhibited high average velocities of $0.8–1.0 \times 10^6$ m/s. Implications in the context of TGF models are discussed. These results paint the first clear picture of the lightning processes that occur before, during, and after TGF production.

1. Introduction

The connection between atmospheric electricity and high-energy physics is unexpectedly strong [*Dwyer et al.*, 2012], particularly in the form of terrestrial gamma-ray flashes (TGFs) [*Fishman and other*, 1994] and associated high-energy electrons [*Dwyer et al.*, 2008], positrons [*Briggs et al.*, 2011], and perhaps neutrons [*Chilingarian et al.*, 2010]. Many of the details of how thunderstorms generate TGFs, the most commonly observed high-energy thunderstorm phenomenon, remain elusive. Although the relativistic runaway electron avalanche (RREA) process [*Gurevich et al.*, 1992] is widely agreed to be the root cause, there are several distinct theories about the conditions in which the RREA process is initiated and develops [*Dwyer*, 2008; *Celestin et al.*, 2012].

Measurements of the environment in which TGFs are produced could provide key information to help distinguish between these and other proposed mechanisms. It is known that at least some TGFs are produced in association with in-cloud (IC) lightning leader propagation [*Shao et al.*, 2010; *Lu et al.*, 2010; *Cummer et al.*, 2011; *Østgaard et al.*, 2013]. The altitude development of the associated leader has been measured for some TGFs [*Shao et al.*, 2010; *Lu et al.*, 2010], and the source altitude of TGFs have been measured in several cases [*Cummer et al.*, 2014]. But timing uncertainties in the measurements have hindered establishing the precise relationship between leader development and TGF production.

Our goal is to measure, as precisely as we can, where and when TGFs are produced relative to the upward propagating negative leader. We first identify a small subset of TGF-associated lightning radio emissions in which the altitude sequence of in-cloud lightning leader pulses that precede and follow the TGF can be measured by analyzing the time difference between signals reflected by the ionosphere and ground [*Smith et al.*, 2004; *Shao et al.*, 2010]. Using gamma-ray data from the Fermi satellite, which provides absolute timing accuracy better than several microseconds, we identify when the TGF is produced relative to the ascending in-cloud lightning leader.

The three TGFs we analyze paint a remarkably consistent picture in which TGFs are produced near the midpoint of the lightning leader development in both time and altitude, which is several kilometers above and several milliseconds after the leader initiation. After the TGF, the lightning leaders continue to ascend for several more kilometers with no dramatic change to their characteristics prior to the TGF. However, the

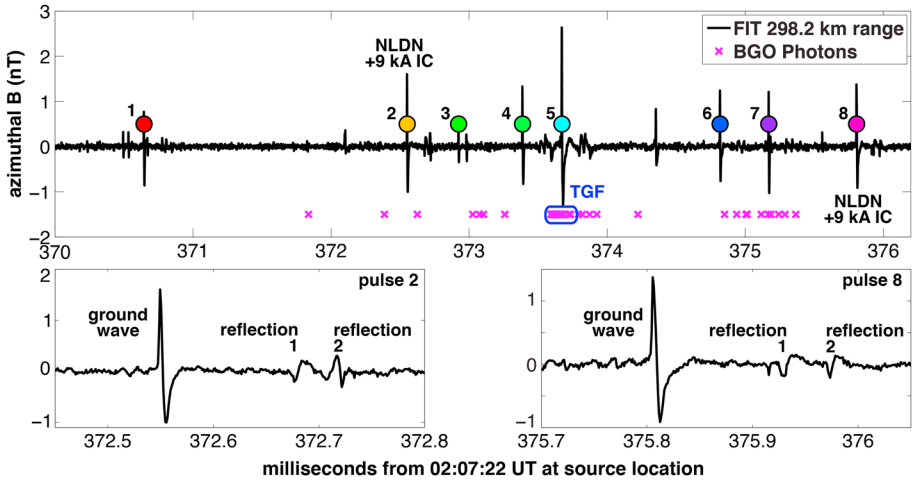

Figure 1. Summary of data for 1 July 2014 TGF. (top) Time-aligned LF radio signal and BGO gamma ray counts, referenced to the source location. The TGF occurred roughly in the middle of eight distinct radio pulses in a 5 ms time window. (bottom row) Zoom-in on the (bottom left) second and (bottom right) eighth radio pulses, showing that two ionospherically reflected pulses are clearly detectable for each ground wave. The relative timing of the reflected pulses reflects the source altitude of each.

average leader propagation velocity is fast and ranges from 0.8 to 1.0 $\times$ 10^6 m/s, and the leader velocities increase with altitude in all three cases. These are atypical leader properties which may reflect an unusually strong background electric field. Regardless, these observations show that TGFs are produced in the middle of one of the most common and ordinary lightning processes on the planet, and it continues to puzzle why they are infrequently observed.

2. Instruments and Data

The TGF photons in the events analyzed here were observed by the Gamma-ray Burst Monitor (GBM) instrument on the Fermi satellite [*Briggs et al.*, 2010] and were identified in the GBM ground search procedure [*Briggs et al.*, 2013]. We focus here solely on the gamma rays detected with the higher-energy (>200 keV) bismuth germanate (BGO) detectors [*Briggs et al.*, 2010] to deemphasize any lower energy Compton-scattered photons and ensure that the duration of the BGO counts reflects the duration of the TGF. The simultaneous radio emissions were recorded with a two-axis low-frequency (LF) magnetic field sensor with a 1–300 kHz bandwidth deployed at the Florida Institute of Technology and located at 28.062°N latitude and −80.624°E longitude. The sensor has a flat frequency response from 100 to 200 kHz and a frequency-proportional response from 1 to 100 kHz. Absolute amplitude calibration was obtained from both laboratory measurements and in-field cross calibration with other magnetic sensors. GPS timing for both the radio and photon measurements ensures absolute timing accuracy of several microseconds.

The TGFs analyzed here were carefully selected for this analysis based on several criteria. First, we require National Lightning Detection Network (NLDN) geolocation of lightning radio pulses within at most a few milliseconds of the TGF so that we have an independent measurement of the source location. Second, we require that the LF radio emissions contain a clear sequence of in-cloud (IC) pulses both before and after the TGF, from which the ionospherically reflected pulse pairs can be analyzed to determine the source altitude of the pulse [*Smith et al.*, 2004]. In practice, the distance from source to radio sensor needs to be less than 1000 km so that the time difference between two ionospherically reflected pulses can be reliably measured. We identified and analyze here three TGFs that occurred in calendar 2014 that met these criteria and contained a sufficient number of distinct pulses to provide a clear picture of the altitude progression.

As an example, Figure 1 summarizes the data for the 1 July 2014 TGF. The signal times have been speed-of-light propagated back to the source location. Figure 1 (top) overlays the FIT radio signal and the gamma ray counts detected by the BGO detector. Eight separate ground wave radio pulses are marked in this sequence, beginning 2.7 ms before the TGF and ending 2.0 ms after the TGF. Two of these pulses were reported by the NLDN as +9 kA cloud pulses. Figure 1 (bottom row) zooms in closely on two of those pulses, showing that the ground

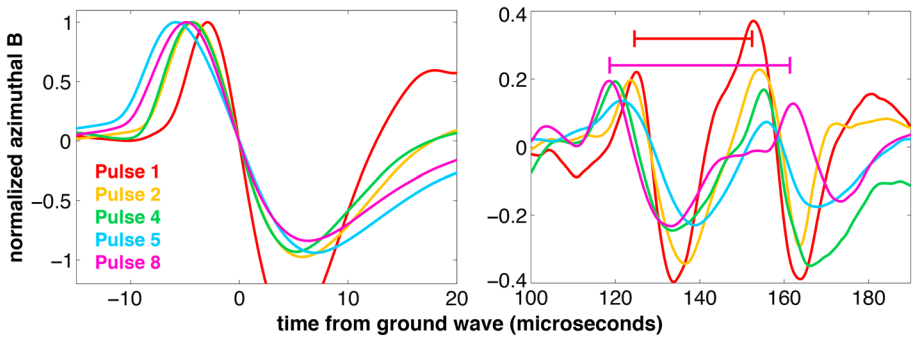

Figure 2. Details of five radio pulses for the 1 July 2014 TGF. (left) Amplitude-normalized ground wave signals, time aligned to the first zero. (right) The ionospherically reflected signal pair for each. The consistent timing relative to the ground wave confirms that these are ionospheric reflections. The time separation between the reflected signals increases detectably with pulse order, confirming the upward ascent of the leader-associated radio source. The time differences for pulse 1 and pulse 8 are explicitly marked.

wave and the ionospherically reflected signal pair can clearly be identified for each. Careful examination shows that the reflected signal pair time difference for pulse 2 is shorter than that for pulse 8, indicating that the former pulse was produced at a lower altitude than the latter pulse [*Smith et al.*, 2004]. This type of pulse sequence is typical of an ascending, negative polarity, in-cloud lightning leader [*Shao and Krehbiel*, 1996]. Throughout this paper, altitudes and lengths refer only to the upward negative polarity portion of the leader. We do not have information about the corresponding downward positive polarity portion of the leader, which does not normally produce strong radio emissions.

3. Data Processing

Our processing approach is straightforward and follows *Smith et al.* [2004]. For each distinct source pulse in the sequence, we measure the times of the first zero crossing of the ground wave signal and of the two reflected signals to 0.1μs precision after upsampling from 1 MHz to 10 MHz sampling. The time difference between the ground wave and the average of the two reflected signals is used to compute the effective ionospheric reflection altitude, using the known NLDN-measured propagation distance. A single average effective reflection altitude is computed from all pulses in each event sequence and used in the subsequent calculations (the reflection altitudes for the individual pulses in a single sequence vary only by a few hundred meters). Then, for each distinct source pulse, the time difference between the two reflected signals is used to estimate the source altitude of the pulse. This purely geometric calculation is performed accounting for the spherical geometry of the system.

To show the feasibility of the approach, Figure 2 overlays five separate pulses from sequence for the 1 July 2014 TGF. The color corresponds to that in Figure 1. Figure 2 (left) shows the amplitude-normalized ground wave signals aligned to a time scale defined by the first zero crossing of the waveform. Figure 2 (right) shows, on the same time scale, the ionospherically reflected signal pair (note that the signals in this panel have been inverted). The critical observation is that the time difference between the two reflected signals increases steadily with pulse order, as expected for an upward ascending lightning leader. The time differences between the reflected signals for the first (red) and last (magenta) pulses in the sequence are marked to show that this time difference increases by approximately 10μs during the leader ascent.

4. Measured Altitude Sequences

This source altitude calculation was performed for the three TGFs in Table 1. Figure 3 shows, for all three events, the measured altitude sequence overlaid on the pulse sequence and the BGO gamma-ray counts. For the 1 July 2014 TGF, the average ground wave to reflection midpoint delay of 144.0μs implies an effective ionospheric reflection height of 81.3 km. The reflected pulse separations increase from 28.6 to 43.2μs, implying source ascent from 9.2 to 13.9 km. This altitude range is almost identical to a TGF-associated leader reported by *Shao et al.* [2010], which helps confirm the validity of our measurements.

Table 1. Details of Analyzed TGFs

Date[a]	TGF Time (UT)	NLDN Location	TGF to LF (km)	TGF to Fermi (km)
2014/07/01	02:07:22	26.17°N, −82.76°E	298	229
2014/08/10	05:49:30	23.87°N, −80.08°E	472	174
2014/09/24	08:35:48	26.52°N, −88.79°E	826	240

[a]Dates are formatted as year/month/day.

The precise absolute photon timing from the GBM instrument enables us, for the first time, to place the TGF precisely in the context of this upward propagating leader. For the 1 July 2014 TGF, as shown in Figure 3 (left), the first pulse in the sequence (which we define throughout as the apparent leader initiation point) occurred 3.0 ms before the median TGF photon and originated at an altitude of 9.2 km. From this apparent leader initiation point, the individual pulses ascend at an average speed of 0.9×10^6 m/s, reaching 13.9 km altitude 5.2 ms after the leader initiation and 2.2 ms after the TGF was produced. The highest altitude pulse before the TGF was from 11.2 km altitude, or 2.0 km above the apparent leader initiation altitude. Note that the pulse closest in time to the TGF was measured to be about 1 km lower than the earlier pulse. This pulse is also significantly of longer duration than all of the others, and it is possible that this difference affects the altitude estimate. An altitude drop is not seen in the leader altitude sequence for the other two TGFs, and we do not think that this necessarily means that the source altitude truly dropped immediately prior to the TGF time.

The resulting altitude sequences for the 10 August 2014 and 24 September 2014 TGFs are shown in Figures 3 (middle) and 3 (right), respectively. The details paint a picture that is remarkably similar for all three TGFs. For the 10 August 2014 TGF, we find an effective ionospheric reflection height of 87.1 km and a leader pulse source altitude that ascended from 7.3 to 11.3 km in 4.0 ms at an average speed of 1.0×10^6 m/s. The NLDN reported the second pulse in the sequence as a +11 kA cloud pulse. The TGF was produced 2.1 ms after apparent initiation of the ascending leader, with a highest preceding source altitude of 8.3 km or 1.0 km above the apparent leader initiation altitude. The leader ascent continued after the TGF for at least 1.9 ms.

For 24 September 2013, we find an effective ionospheric reflection height of 83.1 km, and a pulse source altitude that ascended from 8.0 to 10.7 km in 3.3 ms for an average leader propagation speed of 0.8×10^6 m/s. The NLDN reported one of the large pulses at the time of the TGF as a +118 kA cloud pulse. The TGF was produced 2.2 ms after initiation of the ascending leader, with a highest preceding source altitude of 9.4 km or 1.4 km above the apparent leader initiation altitude. The leader ascent continued after the TGF for at least 1.1 ms.

There are uncertainties in these altitude measurements. The dominant contributor is noise in the measurement of the ionospherically reflected signal pair time difference. For our shortest range event (298 km), a 1 km change in source altitude is produced by a 3.0μs change in time difference. For the longest range event (826 km), a 1 km in source altitude change is produced by a 1.1μs change in time difference. Using zero crossings as time references helps minimize this uncertainty, and from the noise level in the data we estimate

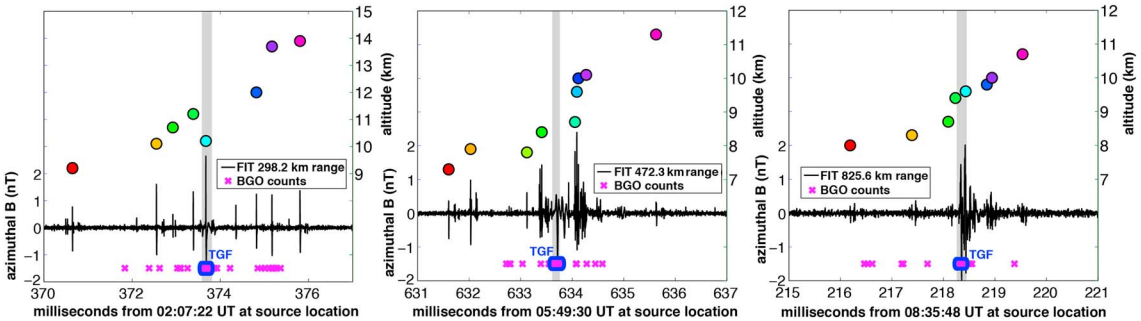

Figure 3. Measured altitude sequence of lightning leader radio pulses overlaid on the radio waveform and the gamma ray counts. (left) For the 1 July 2014 TGF, the lightning leader ascended from 9.2 to 13.9 km altitude in 5.2 ms, and the marked TGF was produced 3.0 ms after lightning initiation. (middle) For the 10 August 2014 TGF, the lightning leader ascended from 7.3 to 11.3 km altitude in 4.0 ms, and the marked TGF was produced 2.1 ms after lightning initiation. (right) For the 24 September 2014 TGF, the lightning leader ascended from 8.0 to 10.7 km altitude in 3.3 ms, and the marked TGF was produced 2.2 ms after lightning initiation.

the time difference measurement uncertainty at approximately 1μs. This corresponds to a 300 m error bar on the 1 July 2014 event and a 1000m error bar on the 24 September 2014 event. This appears to be a conservative error estimate as all three events show the monotonically increasing source altitudes expected from an ascending IC leader, without obvious statistical scatter. *Smith et al.* [2004] found a uniform upward 1 km bias in lightning source altitudes measured with this approach, which could be present here but which would not significantly affect the conclusions. The altitude uncertainty is large enough that the length of any individual step in these sequences is probably not measured with high precision, but the overall leader ascent sequence is clear in each case.

Radar measurements provide additional support for the validity of the leader altitude measurements presented here. Enhanced echo top altitudes of 15.2 km and 12.5 km were measured for the storm cells that produced the 1 July 2014 and 10 August 2014 TGFs, respectively. These altitudes are 1.3 and 1.2 km, respectively, above the highest measured source altitude in each. Radar and lightning mapping array measurements have shown that the upper limits of negative leader propagation can fall 1–2 km short of the 18 dB*Z* enhanced echo top reflectivity [*Wiens et al.*, 2005]. The vertical extent of the leader altitude measurements presented here are thus consistent with simultaneous radar measurements.

In all three cases, the leader continued upward after the TGF with no dramatic changes to its pre-TGF characteristics. All three sequences appear to exhibit a leader velocity that increases with time, with an average post-TGF leader velocity approximately 1.5–2.5 times faster than the average pre-TGF velocity. The velocity appears to increase most rapidly around the time of the TGF, although the individual altitude measurements are not measured with sufficient precision to say this with certainty.

5. Implications and Conclusions

These measurements complete the previously known partial picture of the TGF-lightning relationship [*Shao et al.*, 2010; *Lu et al.*, 2010; *Cummer et al.*, 2011; *Østgaard et al.*, 2013; *Cummer et al.*, 2014] by determining the altitude and time relationship between lightning leader development and TGF generation. In all cases, the TGFs occurred close to the midpoint of the upward leader development in both time and space, and the upward propagation of the upward leader continued after the TGF with no dramatic changes to its characteristics. More quantitatively, these TGFs occurred after the leader had extended 1.5–2.0 km from its initiation point and had taken several steps in 2–3 ms. After the TGFs, the leaders continued to ascend another 1.5–2.5 km. The highest altitude pre-TGF lightning pulses in these three events are at 11.2, 8.3, and 9.4 km altitude. Note that these altitudes reflect the altitude of the leader tip at the time of TGF initiation and not necessarily where the TGF is produced.

These TGF-associated negative leaders propagated for 2.7–4.7 km in 3.3–5.2 ms at an average upward velocity of $0.8–1.0 \times 10^6$ m/s with an average apparent step length of approximately 500 m. This is fast compared to those reported in *Proctor* [1997] (1.3×10^4 to 1.3×10^5 m/s, median 7.5×10^4 m/s) and *Behnke et al.* [2005] (with a median velocity of 1.6×10^5 m/s in the first few milliseconds). The velocities reported here are closer to those in two TGF-associated leaders reported by *Shao et al.* [2010] of $0.4–0.6\times10^6$ m/s. Collectively, these observations indicate that TGF-associated leaders are atypically fast. The leaders observed here also appear to be accelerating, on average, with altitude. The altitude uncertainty of each measured point makes it difficult to assert this without ambiguity, but the apparent acceleration is a feature of all three altitude sequences. Assuming that the net negative leader velocity is potential dependent, as is known for positive leaders [*Bazelyan and Raizer*, 2000], then we would expect the negative leader to accelerate in a uniform background field [*Behnke et al.*, 2005]. It has been reported, however, that decelerating leaders may be more common *Behnke et al.* [2005], although there are examples in the literature of accelerating leaders [*Marshall et al.*, 2013; *Wu et al.*, 2014].

We can thus say that although the TGF-associated upward leaders are in many ways ordinary, they are relatively long, relatively fast, and possibly accelerating with altitude. This suggests the possibility of a strong in-cloud electric field and a high total potential drop between the main charge centers of the storm. It is also possible that conditions not evident from the leader ascent play a role in TGF production. Nevertheless, it continues to puzzle that TGFs are produced during seemingly ordinary in-cloud leader propagation, which is a very common lightning process, and in a wide range of storm types [*Chronis et al.*, 2015], yet appear to be uncommon relative to the global lightning rate [*Briggs et al.*, 2013].

These three TGFs are unambiguously associated with an upward propagating IC leader, and in our experience most TGFs appear to fit this basic template. However, this does not mean that TGFs cannot sometimes occur spontaneously without association with a lightning leader, although no such event has been definitively reported. This clear connection to an existing upward lightning leader fits in the context of two distinct mechanisms that have been proposed for TGF generation. In the feedback-driven relativistic runaway electron avalanche (RREA) model [*Dwyer*, 2012; *Liu and Dwyer*, 2013], charge rearrangement in a propagating leader increases the electric field over a relatively long (several kilometers) region. This initiates the RREA from just one or a few seed electrons, and positron feedback [*Dwyer*, 2003] then creates the large number of seed particles needed to produce a TGF with a brightness of $10^{17}-10^{18}$ runaway electrons [*Dwyer and Smith*, 2005; *Cummer et al.*, 2014]. In the leader-seeded model [*Celestin et al.*, 2012; *Pasko*, 2014], intense but transient electric fields associated with the stepping of a long leader provide the RREA acceleration, and a large number of thermal runaway electrons from the leader provide the needed seed particles. The latter model requires a stepping lightning leader to generate the high-field TGF acceleration region, and in the former model it increases the large-scale electric field and thus drives the TGF acceleration.

Another interesting observation emerges from these measurements in the context of these models. Why are TGFs not produced in earlier or later stages of the same leader? Later stages at higher altitude would aid satellite TGF observability, and the longer and thus higher-potential leader would increase the key electric field in both mechanisms. And earlier stages are not so much at lower altitude that a generated TGF could not be detected by satellite. But multipulse TGFs are only approximately 20% of all TGFs [*Foley and other*, 2014], and the TGFs reported here as well as those known or likely to be associated with upward leaders [*Shao et al.*, 2010; *Lu et al.*, 2010; *Østgaard et al.*, 2013] contained only a single gamma ray pulse. We suggest that this apparent suppression of additional TGFs is a feature that should be explained by TGF models.

In summary, our measurements show definitively that at least some (and perhaps most) TGFs are produced when a relatively long (1–2 km) upward propagating IC leader has developed. Although our observations do not immediately support one TGF generation model over another, they provide a more complete picture of the scenario in which TGFs are produced. Folding this picture into TGF simulations should help answer some of the critical open questions behind the enigmatic physics of TGF generation.

Acknowledgments
The authors would like to acknowledge support from the NASA Fermi Guest Investigator program through grant NNX13AO89G, the National Science Foundation Dynamic and Physical Meteorology program through grants ATM-1047588, and AGS-1519236 Science Foundation Ireland under grant 12/IP/1288, and the DARPA Nimbus program through grants HR0011-10-1-0059 and HR0011-10-1-0061. We thank Eric Cramer (Florida Institute of Technology) for leading the operation of the LF radio sensors used in this work. We thank Ken Cummins (Vaisala, Inc.) for providing lightning geolocation data and analysis. We thank Lisa Gibby (Jacobs Technology), Valerie Connaughton (USRA), Matthew Stanbro (UA Huntsville), and Sheila McBreen (University College Dublin) for quickly finding TGFs in the GBM data. Fermi GBM data are publicly available through the Fermi Science Support Center. LF radio data for the three events analyzed here are available by request (cummer@ee.duke.edu).

The Editor thanks two anonymous reviewers for their assistance in evaluating this paper.

References

Bazelyan, E. M., and Y. P. Raizer (2000), *Lightning Physics and Lightning Protection*, IOP, London.

Behnke, S. A., R. J. Thomas, P. R. Krehbiel, and W. Rison (2005), Initial leader velocities during intracloud lightning: Possible evidence for a runaway breakdown effect, *J. Geophys. Res.*, *110*, D10207, doi:10.1029/2004JD005312.

Briggs, M. S., et al. (2010), First results on terrestrial gamma ray flashes from the Fermi Gamma-ray Burst Monitor, *J. Geophys. Res.*, *115*, A07323, doi:10.1029/2009JA015242.

Briggs, M. S., et al. (2011), Electron-positron beams from terrestrial lightning observed with Fermi GBM, *Geophys. Res. Lett.*, *38*, L02808, doi:10.1029/2010GL046259.

Briggs, M. S., et al. (2013), Terrestrial gamma-ray flashes in the Fermi era: Improved observations and analysis methods, *J. Geophys. Res. Space Physics*, *118*, 3805–3830, doi:10.1002/jgra.50205.

Celestin, S., W. Xu, and V. P. Pasko (2012), Terrestrial gamma ray flashes with energies up to 100 MeV produced by nonequilibrium acceleration of electrons in lightning, *J. Geophys. Res.*, *117*, A05315, doi:10.1029/2012JA017535.

Chilingarian, A., et al. (2010), Ground-based observations of thunderstorm-correlated fluxes of high-energy electrons, gamma rays, and neutrons, *Phys. Rev. D*, *82*, 043009, doi:10.1103/PhysRevD.82.043009.

Chronis, T., et al. (2015), Characteristics of thunderstorms that produce terrestrial gamma-ray flashes, *Bull. Am. Meteorol. Soc.*, doi:10.1175/BAMS-D-14-00239.1, in press.

Cummer, S. A., G. Lu, M. S. Briggs, V. Connaughton, S. Xiong, G. J. Fishman, and J. R. Dwyer (2011), The lightning-TGF relationship on microsecond timescales, *Geophys. Res. Lett.*, *38*, L14810, doi:10.1029/2011GL048099.

Cummer, S. A., M. S. Briggs, J. R. Dwyer, S. Xiong, V. Connaughton, G. J. Fishman, G. Lu, F. Lyu, and R. Solanki (2014), The source altitude, electric current, and intrinsic brightness of terrestrial gamma ray flashes, *Geophys. Res. Lett.*, *41*, 8586–8593, doi:10.1002/2014GL062196.

Dwyer, J. R. (2003), A fundamental limit on electric fields in air, *Geophys. Res. Lett.*, *30*(20), 2055, doi:10.1029/2003GL017781.

Dwyer, J. R. (2008), Source mechanisms of terrestrial gamma-ray flashes, *J. Geophys. Res.*, *113*, D10103, doi:10.1029/2007JD009248.

Dwyer, J. R. (2012), The relativistic feedback discharge model of terrestrial gamma ray flashes, *J. Geophys. Res.*, *117*, A02308, doi:10.1029/2011JA017160.

Dwyer, J. R., and D. M. Smith (2005), A comparison between Monte Carlo simulations of runaway breakdown and terrestrial gamma-ray flash observations, *Geophys. Res. Lett.*, *32*, L22804, doi:10.1029/2005GL023848.

Dwyer, J. R., B. W. Grefenstette, and D. M. Smith (2008), High-energy electron beams launched into space by thunderstorms, *Geophys. Res. Lett.*, *35*, L02815, doi:10.1029/2007GL032430.

Dwyer, J. R., D. M. Smith, and S. A. Cummer (2012), High-energy atmospheric physics: Terrestrial gamma-ray flashes and related phenomena, *Space Sci. Rev.*, *173*, 133–196, doi:10.1007/s11214-012-9894-0.

Fishman, G. J., and other (1994), Discovery of intense gamma-ray flashes of atmospheric origin, *Science*, *264*(5163), 1313–6.

Foley, S., and other (2014), Pulse properties of terrestrial gamma-ray flashes detected by the Fermi Gamma-Ray Burst Monitor, *J. Geophys. Res. Space Physics*, *119*, 5931–5942, doi:10.1002/2014JA019805.

Gurevich, A. V., G. M. Milikh, and R. Roussel-Dupre (1992), Runaway electron mechanism of air breakdown and preconditioning during a thunderstorm, *Phys. Lett. A*, *165*, 463–468.

Liu, N. Y., and J. R. Dwyer (2013), Modeling terrestrial gamma ray flashes produced by relativistic feedback discharges, *J. Geophys. Res. Space Physics*, *118*, 2359–2376, doi:10.1002/jgra.50232.

Lu, G., et al. (2010), Lightning mapping observation of a terrestrial gamma-ray flash, *Geophys. Res. Lett.*, *37*, L11806, doi:10.1029/2009GL038880.

Marshall, T., M. Stolzenburg, S. Karunarathne, S. Cummer, G. Lu, H.-D. Betz, M. Briggs, V. Connaughton, and S. Xiong (2013), Initial breakdown pulses in intracloud lightning flashes and their relation to terrestrial gamma ray flashes, *J. Geophys. Res. Atmospheres*, *118*, 10907, doi:10.1002/jgrd.50866.

Østgaard, N., T. Gjesteland, B. E. Carlson, A. B. Collier, S. A. Cummer, G. Lu, and H. J. Christian (2013), Simultaneous observations of optical lightning and terrestrial gamma ray flash from space, *Geophys. Res. Lett.*, *40*, 2423–2426, doi:10.1002/grl.50466.

Pasko, V. P. (2014), Electrostatic modeling of intracloud stepped leader electric fields and mechanisms of terrestrial gamma ray flashes, *Geophys. Res. Lett.*, *41*, 179–185, doi:10.1002/2013GL058983.

Proctor, D. E. (1997), Lightning flashes with high origins, *J. Geophys. Res.*, *102*, 1693–1706, doi:10.1029/96JD02635.

Shao, X., T. Hamlin, and D. M. Smith (2010), A closer examination of terrestrial gamma-ray flash-related lightning processes, *J. Geophys. Res.*, *115*, A00E30, doi:10.1029/2009JA014835.

Shao, X. M., and P. R. Krehbiel (1996), The spatial and temporal development of intracloud lightning, *J. Geophys. Res.*, *101*, 26,641–26,668, doi:10.1029/96JD01803.

Smith, D. A., M. J. Heavner, A. R. Jacobson, X. M. Shao, R. S. Massey, R. J. Sheldon, and K. C. Wiens (2004), A method for determining intracloud lightning and ionospheric heights from VLF/LF electric field records, *Radio Sci.*, *39*, RS1010, doi:10.1029/2002RS002790.

Wiens, K. C., S. A. Rutledge, and S. A. Tessendorf (2005), The 29 June 2000 supercell observed during STEPS. Part II: Lightning and charge structure, *J. Atmos. Chem. Sci.*, *62*, 4151–4177, doi:10.1175/JAS3615.1.

Wu, T., S. Yoshida, T. Ushio, Z. Kawasaki, and D. Wang (2014), Lightning-initiator type of narrow bipolar events and their subsequent pulse trains, *J. Geophys. Res. Atmos.*, *119*, 7425–7438, doi:10.1002/2014JD021842.